Journal of Engineering Research xxx (xxxx) xxx

Contents lists available at ScienceDirect

Journal of Engineering Research

journal homepage: www.journals.elsevier.com/journal-of-engineering-research

Dynamics and vibrations of mechanically-connected beams system

Abdulaziz Alazmi [a], Abdullah Alshaya [b,*], Khaled Alhazza [b]

[a] Kuwait Oil Company, Kuwait
[b] Mechanical Engineering Department, College of Engineering and Petroleum, Kuwait University, PO Box 5969, Safat 13060, Kuwait

ARTICLE INFO

Keywords:
Connected beams
Mode Shapes
Galerkin's Method
Beam Vibrations

ABSTRACT

An analytical methodology of determining the system frequencies of a mechanically-connected beams system and their corresponding mode shapes is proposed. The methodology is demonstrated by analyzing the mechanical system that is consisted of two cantilever beams coupled by a weak beam. The dynamics of the considered system governed by linear partial differential equations of motion were discretized by means of Galerkin's method into five partial differential equations. Upon applying the mechanical boundary conditions and imposing the continuity constraints which result of twenty boundary conditions, the boundary-value problem (BVP) was significantly reduced to a set of only three linear homogeneous algebraic equations. The latter was only function of three constants and the corresponding system natural frequency. To validate the presented methodology, the analytical results were compared with these obtained numerically using commercial finite element software. Results from the proposed analytical method show an excellent agreement in terms of the mode shapes and natural frequencies with the numerically-predicted results. Furthermore, the effects on the system natural frequencies upon changing the location of coupled weak beam to the two cantilever beam as well as its corresponding length are also investigated.

Introduction

Mechanically-connected beams have recently attracted the attention of many engineers and researchers in many applications such as filters, switches, energy harvesters and structural supports [1,2]. This rises the importance of studying the beams vibrations and dynamics in designing and understanding the static and dynamic responses theoretically, computationally, and experimentally. Even though several numerical methods generated using finite-element packages usually give very accurate (approximate) results of the system natural frequencies and their corresponding mode shapes, they fail to give an insight or an understanding of the problem, and they are constrained by convergence drawbacks and their computational expenses. Therefore, analytical approaches are usually utilized to study beam structures in order to fully understand the dynamics of the structure as well as the effect of each interest parameters. Even though several beam theories were introduced and beams with different support configurations were explored, there have been few attempts in studying the dynamics and vibrations of multi-connected beam structures using continuous (distributed-parameter) systems. Finding the system natural frequencies, the mode shapes, and the equations of motion are crucial in designing and analyzing multi-connected beam structures.

In this work, an analytical methodology of determining the system frequencies as well as their corresponding mode shapes of a mechanically-connected beam in a closed-form expression is presented. It is preferable to study analytically the dynamics and vibrations of multi-connected beam structures in order to have a clear and deeper insight into the relationship among the performance metrics such as boundary conditions and structural material properties, cross-sectional geometry, and overall dimensions. The understanding of these underlying relationships among these metrics helps the engineers in their designing process for such multi-connected beam structures. Furthermore, the analytical expressions can be easily handled compared to the numerical approaches using for instance the finite-element method. Upon deriving the closed-form expression of the system natural frequencies and their mode shapes by developing the reduced-order models of the considered coupled-beam systems, it becomes quite straightforward to determine the effects of one or even more system metrics on the system response as well as to characterize the nonlinear static and dynamic of the structure. These analyses based on the analytical approach are more robust and accurate compared to the numerical techniques.

There are many theories used to describe the behavior of beams;

* Corresponding author.
E-mail addresses: mech.eng04@gmail.com (A. Alazmi), abdullah.alshaye@ku.edu.kw (A. Alshaya), kalhazza@vt.edu (K. Alhazza).

https://doi.org/10.1016/j.jer.2024.11.007
Received 25 July 2024; Received in revised form 19 November 2024; Accepted 19 November 2024
Available online 26 November 2024

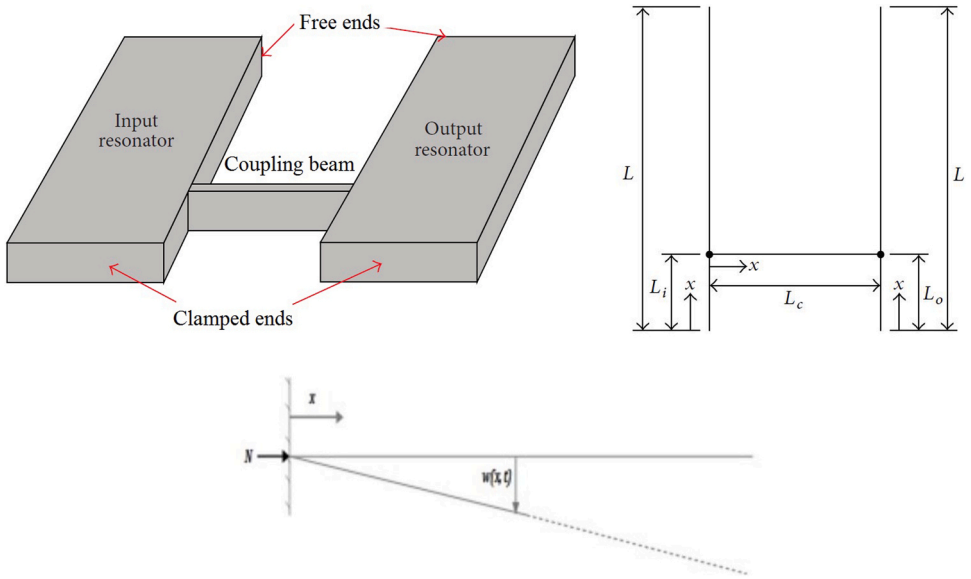

Fig. 1. (a) A schematic drawing, (b) a schematic model of a mechanical system made of two clamped-free beams connected by a weak coupling beam, and (c) a schematic diagram of one of the primary beams.

Euler-Bernoulli beam theory, Timoshenko beam theory, Rayleigh theory, Layerwise theories, … etc [3–6]. The beam theories are usually classified based on the order of the polynomial used in the displacements approximation throughout the beam thickness [2,7,8]. The effect of mid-plane stretching and inertia nonlinearity (i.e., transverse motion curvature of a beam) in transverse vibration of fixed-fixed, simply--supported, and inextensional (with one end is fixed and the other is either free or sliding) beams requires nonlinear theories. The free vibration of a equally-distant simply-supported (hinged ends) are analyzed by Woinowsky-Krieger [9] and Burgreen [10]. Evensen [11] studied the effect of mid-plane stretching on the vibrations of a uniform beam with fixed ends for simply supported, clamped, and clamped-simply supported cases. The geometric and inertia terms are the main contribution of the effective nonlinearity in the beams. Bolotin [12] showed that the nonlinearity effects from the beam inertia are more significant than the nonlinearity effects from the beam geometry, where Atluri [13] showed that the nonlinear effects of the two terms depend on the mode number in axial vibration of a hinged beam whose one end is free.

Upon deriving the analytical expression of nonlinear equations of motion of inextensional isotopic beams in flexural-flexural-torsional motion, Crespo da Silva and Glynn [14,15] showed that the magnitude order of the nonlinearities arising from the geometric curvature are the same with the magnitude order due to the nonlinearities arising from the beam inertia. Furthermore, Pai and Nayfeh [16] considered the nonlinearlity of cantilever beams and demonstrated that the nonlinearity effects due to beam geometry is dominant in the first mode (hardening type), where it is due to beam inertia in the second and higher modes (softening type). Crespo da Silva and Zaretzky [17] studied the nonlinear effects of beams exhibiting pitching and bending in space and derived the corresponding nonlinear equations of motion using variational principle while accounting the nonlinearity effects due to gravity gradient and deformation.

Han et al. [18] investigated the vibration of beams by obtaining the corresponding equations of motions with different supporting conditions: free-free, clamped-clamped, hinged-hinged, and clamped-free beams, while using different beam theories: Euler-Bernoulli theory, Rayleigh theory, shear theory, and Timoshenko theory. Arafat [19] studied the nonlinear and nonplanar steady-state response of a cantilever beam to direct and parametric harmonic excitation using a perturbation technique. Emam [20] extended Galerkin method to a multi-mode system by developing what is known Galerkin discretization model that is capable of analyzing beams and shells systems that possess quadratic and cubic nonlinearities. The concept of the developed discretization model is to reduce the spatial and temporal governing partial differential equations of motion into a set of nonlinearly coupled ordinary-differential equations in a time coordinate only. Malatkar [7] studied the nonlinear vibrations of metallic cantilever beams and plates subjected to transverse harmonic excitation, and observed that the energy transfer between the widely spaced modes is a function of the closeness of modulation frequency to the natural frequency of the first mode.

Hammad [21,22] studied the vibration of mechanically-coupled beam resonators that are clamped at both ends and analytically calculated the natural frequencies, and hence, the mode shapes as well as determined the critical buckling loads. Such application of mechanically-coupled beam resonators is found in micromechanical beam filters. Gurbuz et al. [23] presented a coupling spring design for a microelectromechanical (MEMS) filter that follows mechanical-electrical-mechanical domain. Ding et al. [24] investigated the natural frequency of nonlinear coupled planar vibration for axially moving beams in the supercritical transport speed range. Arora [25] studied experimentally free vibrations of cantilever beams of different materials and compared the results with the ones found using Finite-Element Method (FEM).

Recent advancements have highlighted the improvements in dynamic modeling and natural frequency analysis of connected beam systems, particularly under various boundary conditions and material properties. For instance, Ma et al. [26] developed a dynamic model for rotating laminated beams, considering the foreshortening effect to improve accuracy in resonant speed calculations. Similarly, Kim et al. [27] analyzed the natural frequency of elastically connected double-beam systems using the Haar wavelet method under various boundary conditions, providing new insights into the dynamic response of such systems. Additionally, recent research on functionally graded piezoelectric beams has shown the influence of thermal effects and design parameters on their static and dynamic behavior, which is crucial for understanding smart structure applications [28]. Recent advancements have further explored the nonlinear forced vibration and stability of axially moving beams with internal hinges, employing techniques such as Hamilton's principle and numerical tools like the MatCont toolbox to analyze amplitude-frequency response characteristics under

varying conditions [29].

The influence of external control parameters such as mass perturbation and DC voltage bias has been shown to significantly impact the frequency response and dynamic behavior of mechanically coupled systems. Recent work by Rabenimanana et al. (2022) investigates the equivalence between mass perturbation and DC voltage bias in coupled MEMS resonators, revealing that small changes in the DC voltage can produce shifts in natural frequency similar to those induced by mass changes. This provides a new perspective on the inherent nonlinear effects and suggests practical applications in mass sensing, without requiring the complexities of mass deposition. This insight can be beneficial for the development of enhanced sensitivity in coupled beam structures through control of external actuation parameters, aligning with the need for improved dynamic modeling and response analysis in multi-connected beam systems [30]. Recent advancements in MEMS resonator-based mass sensing techniques have demonstrated significant improvements in sensitivity and robustness. For instance, Najar et al. [31] developed a multi-physics model of an electrostatic MEMS resonator consisting of an array of mechanically-coupled beams and investigated its use for mass detection. The study demonstrated that incorporating a differential capacitive sensing mechanism, along with electrostatic actuation, enhances sensitivity significantly by leveraging mode localization and nonlinear effects, such as bifurcation and softening, to detect mass perturbations precisely. These advancements are particularly relevant to our study of mechanically connected beams, as they offer promising approaches to improve mass sensitivity in similar coupled systems.

Although Hammad [21,22] proposed a closed-form expressions of the natural frequencies and mode shapes for mechanically-coupled clamped-clamped beams via a weak beam, this work considers a mechanically-coupled system that is consisted of clamped-free beams connected via a weak beam. The problem formulation utilizes the theories corresponding to the continuous (distributed-parameter) system. In the following sections, the governing equations of the linear vibration problem were derived with the associated boundary conditions. The corresponding eigenvalue problem was discussed and manipulated to reduce the system order from which the natural frequencies and mode shapes were computed. The obtained results were then validated using commercial finite element software (ANSYS and COMSOL). In addition, the effects on the system natural frequencies upon changing the location of coupled weak beam to the two cantilever beam as well as its corresponding length are also investigated and studied.

Problem formulation

Consider a mechanical system that is shown in Fig. 1(a) which consists of two clamped-free cantilever beam resonators, also known as the primary beams, whose lengths, L, are equal. The two beams are coupled via a third weak beam, referred to as coupling beam, whose length is L_c. The coupling of the weak beam to the two primary beams divides the latter into two parts as shown in Fig. 1(b). The first and second parts of each of the primary beams will be distinguished by the subscripts 1 and 2, respectively. The left primary beam is referred to as the input beam and will be designated using the subscript i, where the right primary beam is referred to as the output beam and will be designated using the subscript o. The subscript c refers to quantities related to the coupling beam. The beams are referred to as input and output resonators because they function as components of a microelectromechanical system (MEMS) filter. The input resonator receives the mechanical or vibrational signal, and the output resonator delivers the filtered signal. This design specifically targets microfilter applications, where frequency selectivity and signal modulation are critical. The mechanically-coupled beams system allows for efficient signal filtering, which is essential for applications in MEMS RF filters and other communication systems. The spatial coordinates, x, starts at the clamped end, i.e., $x = 0$, and ends at the free end, i.e., $x = L$. As depicted in Fig. 1(b), the primary resonators are coupled by the coupling beam at the corresponding spatial locations $x = L_i$ and $x = L_o$ for input i and output o beams, respectively.

Upon utilizing the Hamilton/Lagrangian principle, the equations of motion of the mechanical system in Fig. 1(a) that describes its dynamics and vibrations will constitute of five partial differential equations (each parts of the primary beams governs by one equation of motion and one for the coupling beam) [32]. The enforcement of clamped and free boundary conditions at both ends of the primary beams will result of eight constraints (four boundary constraints for each primary beams), and the imposing of continuity conditions in terms of deflection, slope, and moment at the coupling positions will result of twelve constraints. The resulting boundary-value problem (BVP) will then be transformed by means of Galerkin's method into a system of twenty linear homogeneous algebraic equations with twenty unknown constants and the system natural frequency. The latter will be further reduced to a set of only three linear homogeneous algebraic equations with three unknown constants and the system natural frequency. Upon enforcing singularity behavior of the resulting coefficient matrix of the reduced problem to avoid having trivial solution, the characteristic equation can be obtained through setting the determinant of the matrix to zero, and hence, one can determine the natural frequencies and the mode shapes of the considered mechanical system, Fig. 1.

Governing equations

The Euler-Bernoulli beam theory is utilized here to derive the governing equations of motion for the mechanical system, Fig. 1. The free vibration responses of the lateral displacements, assuming linear undamped behavior, for each segments of the primary beams as well as the coupling beams are governed by the following five partial differential equations,

$$EI\frac{\partial^4 w_{i,1}}{\partial x^4} + \overline{N}_i\frac{\partial^2 w_{i,1}}{\partial x^2} + \rho A\frac{\partial^2 w_{i,1}}{\partial t^2} = 0, \quad \text{for } 0 < x < L_i \tag{1a}$$

$$EI\frac{\partial^4 w_{i,2}}{\partial x^4} + \overline{N}_i\frac{\partial^2 w_{i,2}}{\partial x^2} + \rho A\frac{\partial^2 w_{i,2}}{\partial t^2} = 0, \quad \text{for } L_i < x < L \tag{1b}$$

$$EI\frac{\partial^4 w_{o,1}}{\partial x^4} + \overline{N}_o\frac{\partial^2 w_{o,1}}{\partial x^2} + \rho A\frac{\partial^2 w_{o,1}}{\partial t^2} = 0, \quad \text{for } 0 < x < L_o \tag{1c}$$

$$EI\frac{\partial^4 w_{o,2}}{\partial x^4} + \overline{N}_o\frac{\partial^2 w_{o,2}}{\partial x^2} + \rho A\frac{\partial^2 w_{o,2}}{\partial t^2} = 0, \quad \text{for } L_o < x < L \tag{1d}$$

$$EI_c\frac{\partial^4 w_c}{\partial x^4} + \overline{N}_c\frac{\partial^2 w_c}{\partial x^2} + \rho A_c\frac{\partial^2 w_c}{\partial t^2} = 0, \quad \text{for } 0 < x < L_c \tag{1e}$$

where x is the spatial coordinate (position) defined along each of the beams' axis, Fig. 1(b) and (c); t is the temporal coordinate (time); $w(x, t)$ is transverse deflection of the beam; E is the Young's modulus; I is the cross-sectional second moments of inertia of the beams; ρ is the material density; A is the cross-sectional areas of the beams; $x = L_i$ and $x = L_o$ are the coordinates (locations) where the input, i, and output, o, primary beams are coupled with the weak beam; L is the corresponding length of the input and output primary beam; L_c is the corresponding length of the coupling beam; and $\overline{N}_i$, $\overline{N}_o$, and $\overline{N}_o$ are the applied compressive axial forces in the primary input, primary output, and coupling beams, respectively.

For convenience, the following nondimensional variables are introduced:

$$\begin{aligned} \widehat{w} &= \frac{w}{L}, \quad \widehat{x} = \frac{x}{L}, \quad \widehat{t} = \frac{t}{T}, \\ l_i &= \frac{L_i}{L}, \quad l_o = \frac{L_o}{L}, \quad l_c = \frac{L_c}{L}, \\ N_i &= \frac{\overline{N}_i L^2}{EI}, \quad N_o = \frac{\overline{N}_o L^2}{EI}, \quad N_c = \frac{\overline{N}_c L^2}{EI_c}, \end{aligned} \tag{2}$$

where the time T is given by $T = \sqrt{\rho AL^4/EI}$ and has a unit of second. Upon substituting of Eq. (2) into the equations of motion, Eq. (1), one can obtain the following nondimensional partial differential equations (after dropping the hats),

$$\frac{\partial^4 w_{i,1}}{\partial x^4} + N_i \frac{\partial^2 w_{i,1}}{\partial x^2} + \frac{\partial^2 w_{i,1}}{\partial t^2} = 0, \quad \text{for } 0 < x < l_i \tag{3a}$$

$$\frac{\partial^4 w_{i,2}}{\partial x^4} + N_i \frac{\partial^2 w_{i,2}}{\partial x^2} + \frac{\partial^2 w_{i,2}}{\partial t^2} = 0, \quad \text{for } l_i < x < 1 \tag{3b}$$

$$\frac{\partial^4 w_{o,1}}{\partial x^4} + N_o \frac{\partial^2 w_{o,1}}{\partial x^2} + \frac{\partial^2 w_{o,1}}{\partial t^2} = 0, \quad \text{for } 0 < x < l_o \tag{3c}$$

$$\frac{\partial^4 w_{o,2}}{\partial x^4} + N_o \frac{\partial^2 w_{o,2}}{\partial x^2} + \frac{\partial^2 w_{o,2}}{\partial t^2} = 0, \quad \text{for } l_o < x < 1 \tag{3d}$$

$$\frac{\partial^4 w_c}{\partial x^4} + N_c \frac{\partial^2 w_c}{\partial x^2} + \left(\frac{h}{h_c}\right)^2 \frac{\partial^2 w_c}{\partial t^2} = 0, \quad \text{for } 0 < x < l_c \tag{3e}$$

where h is the beam thickness. The subscript c in h_c states that h_c is the corresponding thickness of the coupling beam.

Boundary conditions

For the fixed (clamped) beam support at $x = 0$, the transverse deflection and slope vanish where, on the other hand, the shear force and bending moment are unrestricted. Furthermore, the transverse deflection and slope are unrestricted at the beam free-end support, $x = 1$ (at the physical location of $x = L$), where the shear force and bending moment vanish. Therefore, the boundary conditions can be stated as,

$$w_{i,1}(0,t) = 0, \quad \frac{\partial w_{i,1}}{\partial x}\Big|_{x=0} = 0, \quad w_{o,1}(0,t) = 0, \quad \frac{\partial w_{o,1}}{\partial x}\Big|_{x=0} = 0 \quad \text{Fixed-end} \tag{4a}$$

$$\frac{\partial^2 w_{i,2}}{\partial x^2}\Big|_{x=1} = 0, \quad \frac{\partial^3 w_{i,2}}{\partial x^3}\Big|_{x=1} = 0, \quad \frac{\partial^2 w_{o,2}}{\partial x^2}\Big|_{x=1} = 0, \quad \frac{\partial^3 w_{o,2}}{\partial x^3}\Big|_{x=1} = 0 \quad \text{Free-end} \tag{4b}$$

At the attachment points of the input and output primary beams with the coupling beam, $x = l_i$ and $x = l_o$ (at the physical locations of $x = L_i$ and $x = L_o$), the continuity of deflection, slope, and moment holds. Therefore, the continuity conditions can be stated as,

$$w_{i,1}(l_i,t) = w_{i,2}(l_i,t), \quad \frac{\partial w_{i,1}}{\partial x}\Big|_{x=l_i} = \frac{\partial w_{i,2}}{\partial x}\Big|_{x=l_i}, \quad \frac{\partial^2 w_{i,1}}{\partial x^2}\Big|_{x=l_i} = \frac{\partial^2 w_{i,2}}{\partial x^2}\Big|_{x=l_i} \tag{5a}$$

$$w_{o,1}(l_o,t) = w_{o,2}(l_o,t), \quad \frac{\partial w_{o,1}}{\partial x}\Big|_{x=l_o} = \frac{\partial w_{o,2}}{\partial x}\Big|_{x=l_o}, \quad \frac{\partial^2 w_{o,1}}{\partial x^2}\Big|_{x=l_o} = \frac{\partial^2 w_{o,2}}{\partial x^2}\Big|_{x=l_o} \tag{5b}$$

Similarly, the coupling beam deflections, $w_c(0, t)$ and $w_c(l_c, t)$, at the attachment points $x = 0$ and $x = l_c$ (in terms of the spatial coordinate corresponding the coupling beam axis, $x = 0$ and $x = L_c$) should equal to the corresponding deflections of the input and output primary beams at their attachment points, $x = l_i$ and $x = l_o$ with their respect to beam axis coordinate. Furthermore, the slope of the coupling beam deflection at the attachment points $x = 0$ and $x = l_c$ should vanish. Therefore, these conditions can be stated as,

$$w_c(0,t) = w_{i,1}(l_i,t), \quad w_c(l_c,t) = w_{o,1}(l_o,t), \quad \frac{\partial w_c}{\partial x}\Big|_{x=0} = 0, \quad \frac{\partial w_c}{\partial x}\Big|_{x=l_c} = 0 \tag{6}$$

Finally, the resultant shear forces in the coupling beam at the beginning, $x = 0$, and the end, $x = l_c$, should equal to the induced changes of the shear forces in the primary input, $x = l_i$, and output, $x = l_o$, beams, respectively. These statements yield to the following conditions,

$$\frac{\partial^3 w_{i,1}}{\partial x^3}\Big|_{x=l_i} - \frac{\partial^3 w_{i,2}}{\partial x^3}\Big|_{x=l_i} = \frac{I_c}{I}\frac{\partial^3 w_c}{\partial x^3}\Big|_{x=0}, \quad \frac{\partial^3 w_{o,1}}{\partial x^3}\Big|_{x=l_o} - \frac{\partial^3 w_{o,2}}{\partial x^3}\Big|_{x=l_o} = -\frac{I_c}{I}\frac{\partial^3 w_c}{\partial x^3}\Big|_{x=l_c} \tag{7}$$

where I and I_c are the cross-sectional moments of inertia of the primary and coupling beams, respectively.

Eigenvalue problem

Natural frequencies

The equations of motion, Eqs. (3), can be solved using the separation of variables method. The solutions of the lateral displacements will assume to be consisted of a spatial function $\phi(x)$ that corresponds to the mode shape of the considered beam and a temporal harmonic function $e^{j\omega t}$ where ω is the nondimensional natural frequency corresponding to these mode shapes, namely

$$w_{i,1}(x,t) = \phi_{i,1}(x)e^{j\omega t}, \quad \text{for } 0 < x < l_i \tag{8a}$$

$$w_{i,2}(x,t) = \phi_{i,2}(x)e^{j\omega t}, \quad \text{for } l_i < x < 1 \tag{8b}$$

$$w_{o,1}(x,t) = \phi_{o,1}(x)e^{j\omega t}, \quad \text{for } 0 < x < l_o \tag{8c}$$

$$w_{o,2}(x,t) = \phi_{o,2}(x)e^{j\omega t}, \quad \text{for } l_o < x < 1 \tag{8d}$$

$$w_c(x,t) = \phi_c(x)e^{j\omega t}, \quad \text{for } 0 < x < l_c \tag{8e}$$

Substitution of the general solution of the beam transverse displacements, Eqs. (8), into the mechanical system equations of motion, Eqs. (3), yields the following ordinary differential equations in the spacial (mode shapes) functions,

$$\phi_{i,1}^{iv}(x) + N_i\phi''(x) - \omega^2\phi_{i,1}(x) = 0, \quad \text{for } 0 < x < l_i \tag{9a}$$

$$\phi_{i,2}^{iv}(x) + N_i\phi''(x) - \omega^2\phi_{i,2}(x) = 0, \quad \text{for } l_i < x < 1 \tag{9b}$$

$$\phi_{o,1}^{iv}(x) + N_o\phi''(x) - \omega^2\phi_{o,1}(x) = 0, \quad \text{for } 0 < x < l_o \tag{9c}$$

$$\phi_{o,2}^{iv}(x) + N_o\phi''(x) - \omega^2\phi_{o,2}(x) = 0, \quad \text{for } l_o < x < 1 \tag{9d}$$

$$\phi_c^{iv}(x) + N_c\phi''(x) - \left(\frac{h}{h_c}\right)^2\omega^2\phi_c(x) = 0, \quad \text{for } 0 < x < l_c \tag{9e}$$

In order to solve the previous ordinary differential equations, the boundary conditions, Eqs. (4) through (7), should be written in terms of the spatial function $\phi(x)$. Upon direct substitution of Eq. (8), the boundary conditions of the primary beams at the clamped and free supports, Eqs. (4), can be restated as

$$\phi_{i,1}(0) = 0, \quad \phi'_{i,1}(0) = 0, \quad \phi_{o,1}(0) = 0, \quad \phi'_{o,1}(0) = 0 \quad \text{Fixed-end} \tag{10a}$$

$$\phi''_{i,2}(1) = 0, \quad \phi'''_{i,2}(1) = 0, \quad \phi''_{o,2}(1) = 0, \quad \phi'''_{o,2}(1) = 0 \quad \text{Free-end} \tag{10b}$$

the continuity conditions in terms of deflection, slope, and moment in the primary beams at the attachment points, Eqs. (5), can be restated as

$$\phi_{i,1}(l_i) = \phi_{i,2}(l_i), \quad \phi'_{i,1}(l_i) = \phi'_{i,2}(l_i), \quad \phi''_{i,1}(l_i) = \phi''_{i,2}(l_i) \tag{11a}$$

Table 1
Specifications of the mechanically-connected beam of Fig. 1 from reference [21, 22].

Beam	Length, $L(\mu m)$	Width, $b(\mu m)$	thickness, $h(\mu m)$
Primary beam	40.80	8.00	1.90
Coupling beam	20.35	0.75	1.90

$$\phi_{o,1}(l_o) = \phi_{o,2}(l_o), \quad \phi'_{o,1}(l_o) = \phi'_{o,2}(l_o), \quad \phi''_{o,1}(l_o) = \phi''_{o,2}(l_o) \tag{11b}$$

the continuity conditions in terms of deflection and slope in the coupling beam at the attachment points, Eqs. (6), can be restated as

$$\phi_c(0) = \phi_{i,1}(l_i), \quad \phi_c(l_c) = \phi_{o,1}(l_o) \tag{12a}$$

$$\phi'_c(0) = 0, \quad \phi'_c(l_c) = 0 \tag{12b}$$

and the conditions of the resultant shear forces in the coupling beam with respect to the induced changes of the shear forces in the primary beams, Eqs. (7), can be restated as

$$\phi'''_{i,1}(l_i) - \phi'''_{i,2}(l_i) = \frac{I_c}{I}\phi'''_c(0) \tag{13a}$$

$$\phi'''_{o,1}(l_o) - \phi'''_{o,2}(l_o) = -\frac{I_c}{I}\phi'''_c(l_c) \tag{13b}$$

It is worthwhile to mention that the order of each of the ordinary differential equations in Eqs. (9) is four, and hence, the general solution for each of the five differential equations will consists of four unknown constants, i.e., a total of twenty constants for the five the differential equations. On the other hand, there are twenty constraints in terms of boundary and continuity conditions to be imposed, Eqs. (10) to (13).

Assuming a general solution of the form of $\phi(x) = a\exp(\beta x)$, the general solutions of Eqs. (8) are

$$\phi_{i,1}(x) = C_1\cos[\beta_{i1}x] + C_2\sin[\beta_{i1}x] + C_{1a}\cosh[\beta_{i2}x] + C_{2a}\sinh[\beta_{i2}x], \quad \text{for } 0 < x < l_i \tag{14a}$$

$$\phi_{i,2}(x) = C_3\cos[\beta_{i1}(1-x)] + C_4\sin[\beta_{i1}(1-x)] + C_{3a}\cosh[\beta_{i2}(1-x)] + C_{4a}\sinh[\beta_{i2}(1-x)], \text{for } l_i < x < 1 \tag{14b}$$

Table 2
Natural frequencies (in MHz) of the mechanically-connected beams system in Fig. 1.

Mode shape #	Natural Frequency		
	Analytical	ANSYS (Difference in %)	COMSOL (Difference in %)
1	1.489	1.514 (1.69)	1.515 (1.73)
2	1.490	1.516 (1.71)	1.517 (1.78)
3	9.328	9.413 (0.92)	9.414 (0.93)
4	9.336	9.423 (0.93)	9.425 (0.95)
5	26.025	25.868 (0.6)	25.840 (0.70)
6	26.109	26.122 (0.05)	26.132 (0.09)

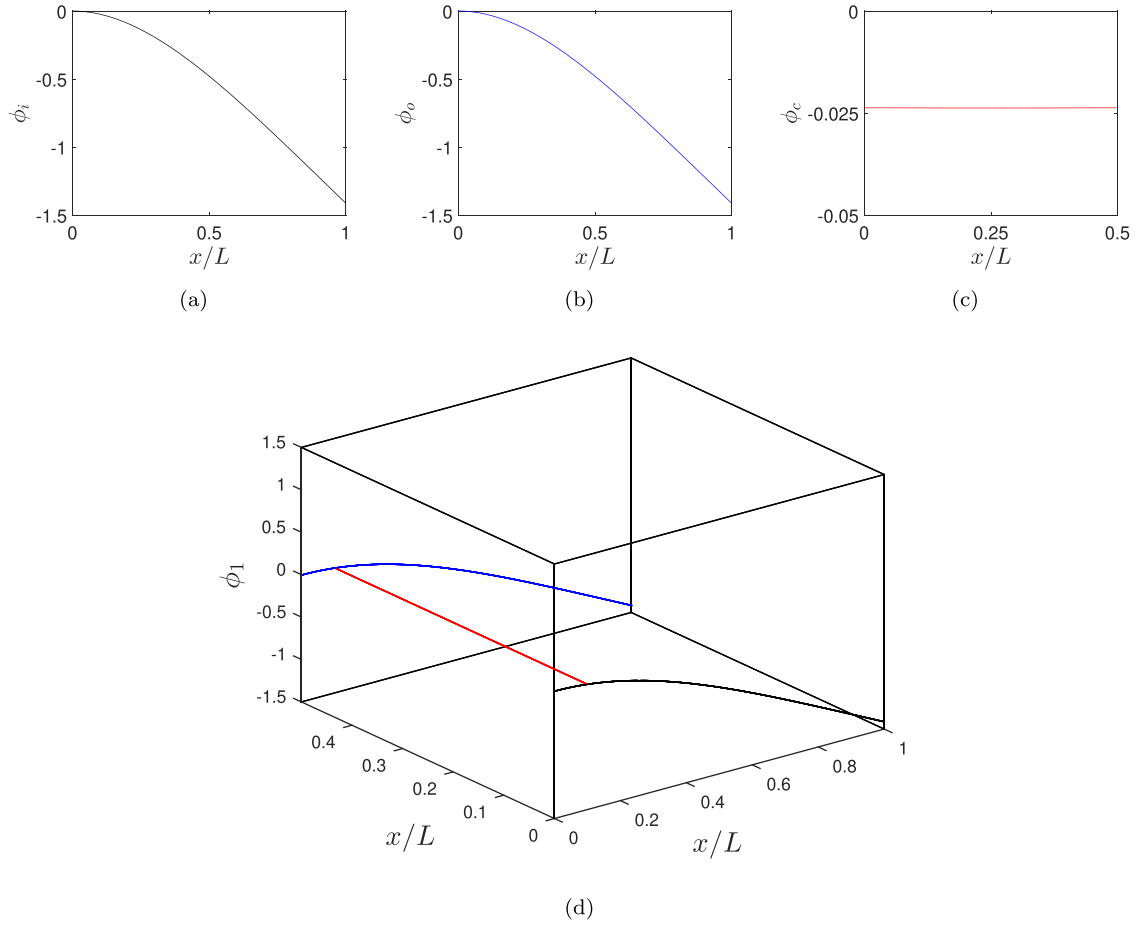

Fig. 2. First mode shape of the mechanically-connected beams system of Fig. 1: mode shape of the (a) primary input beam, (b) primary output beam, (c) coupling beam, and (d) whole mechanical structure.

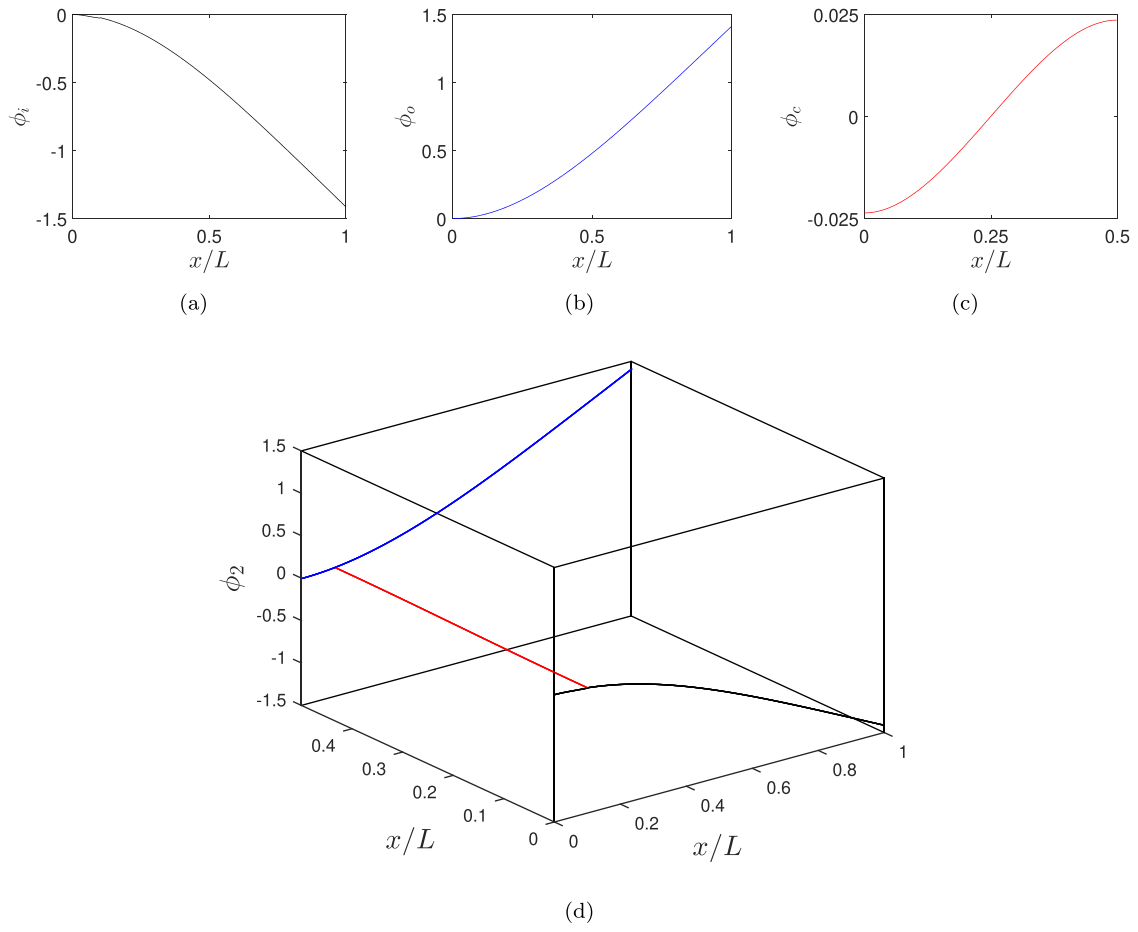

Fig. 3. Second mode shape of the mechanically-connected beams system of Fig. 1: mode shape of the (a) primary input beam, (b) primary output beam, (c) coupling beam, and (d) whole mechanical structure.

$$\phi_{o,1}(x) = C_5\cos[\beta_{o1}x] + C_6\sin[\beta_{o1}x] + C_{5a}\cosh[\beta_{o2}x] + C_{6a}\sinh[\beta_{o2}x], \quad \text{for } 0 < x < l_o \tag{14c}$$

$$\phi_{o,2}(x) = C_7\cos[\beta_{o1}(1-x)] + C_8\sin[\beta_{o1}(1-x)] + C_{7a}\cosh[\beta_{o2}(1-x)] + C_{8a}\sinh[\beta_{o2}(1-x)], \quad \text{for } l_o < x < 1 \tag{14d}$$

$$\phi_c(x) = C_9\cos[\beta_{c1}x] + C_{10}\sin[\beta_{c1}x] + C_{11}\cosh[\beta_{c2}x] + C_{12}\sinh[\beta_{c2}x], \quad \text{for } 0 < x < l_c \tag{14e}$$

where C_1, C_2, …, C_{12}, C_{1a}, C_{2a}, …, C_{8a} are the unknown coefficients to be determined from the boundary and continuity conditions, and the constants β's are given by

$$\beta_{i1} = \sqrt{+\frac{N_i}{2} + \frac{1}{2}\sqrt{N_i^2 + 4\omega^2}}, \quad \beta_{i2} = \sqrt{-\frac{N_i}{2} + \frac{1}{2}\sqrt{N_i^2 + 4\omega^2}} \tag{15a}$$

$$\beta_{o1} = \sqrt{+\frac{N_o}{2} + \frac{1}{2}\sqrt{N_o^2 + 4\omega^2}}, \quad \beta_{i2} = \sqrt{-\frac{N_o}{2} + \frac{1}{2}\sqrt{N_o^2 + 4\omega^2}} \tag{15b}$$

$$\beta_{c1} = \sqrt{+\frac{N_c}{2} + \frac{1}{2}\sqrt{N_c^2 + 4\left(\frac{h}{h_c}\right)^2\omega^2}}, \quad \beta_{c2} = \sqrt{-\frac{N_c}{2} + \frac{1}{2}\sqrt{N_c^2 + 4\left(\frac{h}{h_c}\right)^2\omega^2}} \tag{15c}$$

Imposing the conditions of Eqs. (10) through (13) into the general solution of the spatial functions, Eqs. (14), leads to a linear homogeneous system of twenty algebraic equations. The resultant system can be written in a matrix form as

$$\mathbf{MC} = \mathbf{0} \tag{16}$$

where $\mathbf{M} \in \mathbb{R}^{20\times 20}$ is the coefficient matrix, $\mathbf{C} \in \mathbb{R}^{20\times 1}$ is a vector containing the unknown coefficients (C_1, C_2, …, C_{12} and C_{1a}, C_{2a}, …, C_{8a}), and $\mathbf{0} \in \mathbb{R}^{20\times 1}$ is a zero vector. The elements of the coefficient matrix $\mathbf{M}$ are functions of the mechanical structure dimensions as well as the system natural frequency impeded in the constants β.

Reduction of the eigenvalue problem

To avoid having trivial solution, i.e., $\mathbf{C} = \mathbf{0}$ of Eq. (16), the coefficient matrix $\mathbf{M}$ should be singular, i.e., its determinant should equal to zero. To have a clear and deeper insight into the relationship among the system unknowns as well as to reduce the complexity and the cost when generating the determinant of the coefficient matrix $\mathbf{M}$, Eqs. (14) were analytically manipulated to reduce the number of unknown coefficients. Upon satisfying the boundary conditions of Eqs. (10), the constants C_{ja}

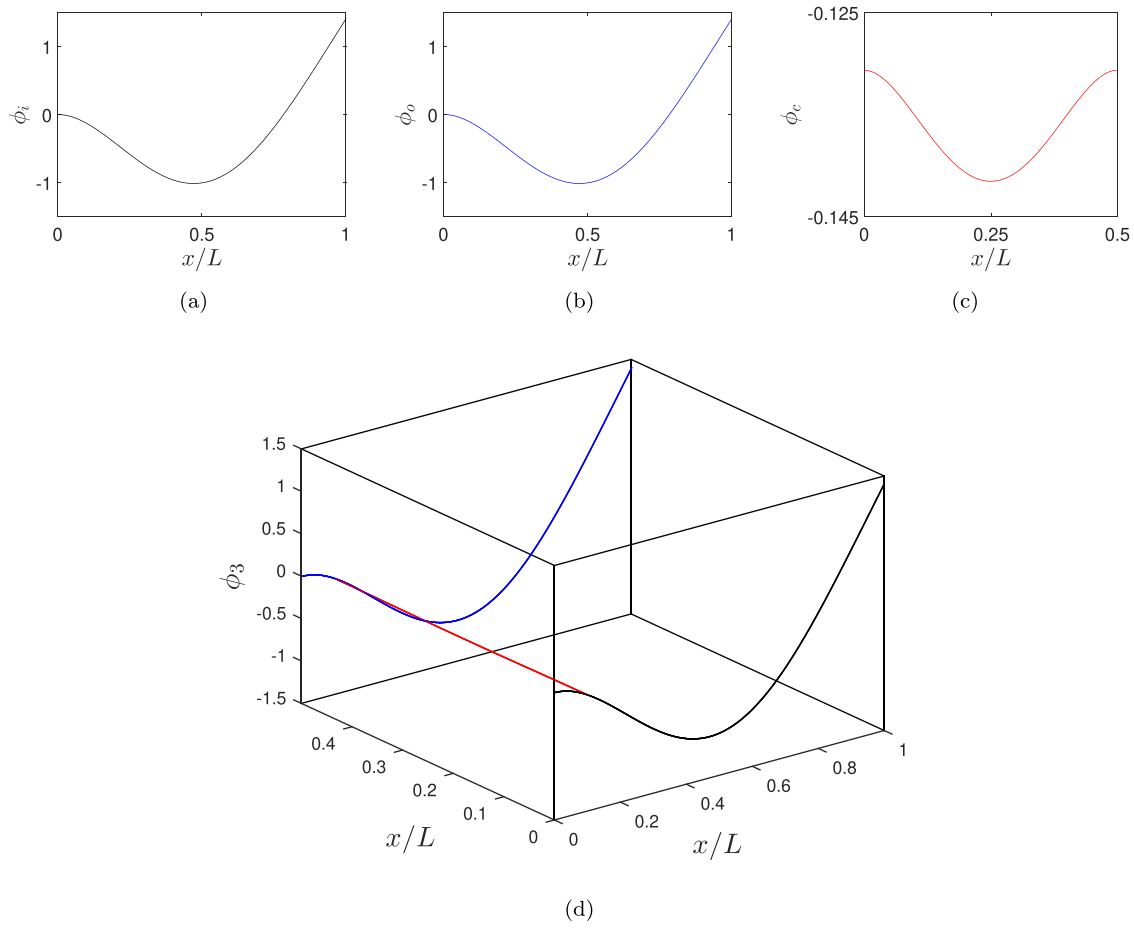

Fig. 4. Third mode shape of the mechanically-connected beams system of Fig. 1: mode shape of the (a) primary input beam, (b) primary output beam, (c) coupling beam, and (d) whole mechanical structure.

can be written in terms of the constants C_j. Hence, Eq. (14) can be rewritten as,

$$\phi_{i,1}(x) = C_1\{\cos[\beta_{i1}x] - \cosh[\beta_{i2}x]\} + C_2\{\sin[\beta_{i1}x] - \sinh[\beta_{i2}x]\}, \quad \text{for } 0 < x < l_i \tag{17a}$$

$$\phi_{i,2}(x) = C_3\{\cos[\beta_{i1}(1-x)] - \cosh[\beta_{i2}(1-x)]\} + C_4\{\sin[\beta_{i1}(1-x)] - \sinh[\beta_{i2}(1-x)]\}, \quad \text{for } l_i < x < 1 \tag{17b}$$

$$\phi_{o,1}(x) = C_5\{\cos[\beta_{o1}x] - \cosh[\beta_{o2}x]\} + C_6\{\sin[\beta_{o1}x] - \sinh[\beta_{o2}x]\}, \quad \text{for } 0 < x < l_o \tag{17c}$$

$$\phi_{o,2}(x) = C_7\{\cos[\beta_{o1}(1-x)] - \cosh[\beta_{o2}(1-x)]\} + C_8\{\sin[\beta_{o1}(1-x)] - \sinh[\beta_{o2}(1-x)]\}, \quad \text{for } l_o < x < 1 \tag{17d}$$

$$\phi_c(x) = C_9\cos[\beta_{c1}x] + C_{10}\sin[\beta_{c1}x] + C_{11}\cosh[\beta_{c2}x] + C_{12}\sinh[\beta_{c2}x], \quad \text{for } 0 < x < l_c \tag{17e}$$

This reduces the number of the unknown constants from twenty constants to twelve constants. Substitution of Eqs. (17) into (11a), (11b), (12b) and (13) a results of nine equations for the C_j to be solved in terms of the constants C_1, C_5, and C_9 [32]. The latter constants correspond to the input, output, and coupling beams, respectively. The imposing of the remaining three conditions, (12a) and (13)b, yields the following reduced problem

$$\mathbf{M_r C}_r = \mathbf{0} \tag{18}$$

where $\mathbf{M_r} \in \mathbb{R}^{3\times3}$ is known as the reduced coefficient matrix and the vector $\mathbf{C}_r \in \mathbb{R}^{3\times1}$ contains the three unknown constants, C_1, C_5, and C_9, namely

$$\mathbf{M_r} = \begin{bmatrix} g_{11} & g_{12} & g_{13} \\ g_{21} & g_{22} & g_{23} \\ g_{31} & g_{32} & g_{33} \end{bmatrix}, \qquad \mathbf{C_r} = \begin{Bmatrix} C_1 \\ C_5 \\ C_9 \end{Bmatrix} \tag{19}$$

where the elements g_{mn} for m, n = 1, 2, 3 are functions of the system natural frequency ω that impeded in the constants β, Eqs. (15), and the zero vector, in this case, is $\mathbf{0} \in \mathbb{R}^{3\times1}$. The characteristic equation of the mechanical system from which the natural frequencies can be determined is obtained by setting the determinant of the reduced coefficient matrix $\mathbf{M_r}$ equal to zero, i.e., $\det[\mathbf{M_r}] = 0$.

Mode shapes of the mechanically-connected beams

The resultant transcendental equation when setting $\det[\mathbf{M_r}] = 0$ has infinite solutions of ω, and for each solution, ω_n, there is a corresponding mode shape. The latter can be obtained by directly substituting the value of ω_n into Eq. (15) to obtain the corresponding numerical values of β's, where these β's values were substituted into Eq. (17). Finally, numerical relations among the unknown constants when imposing the boundary conditions will end up with

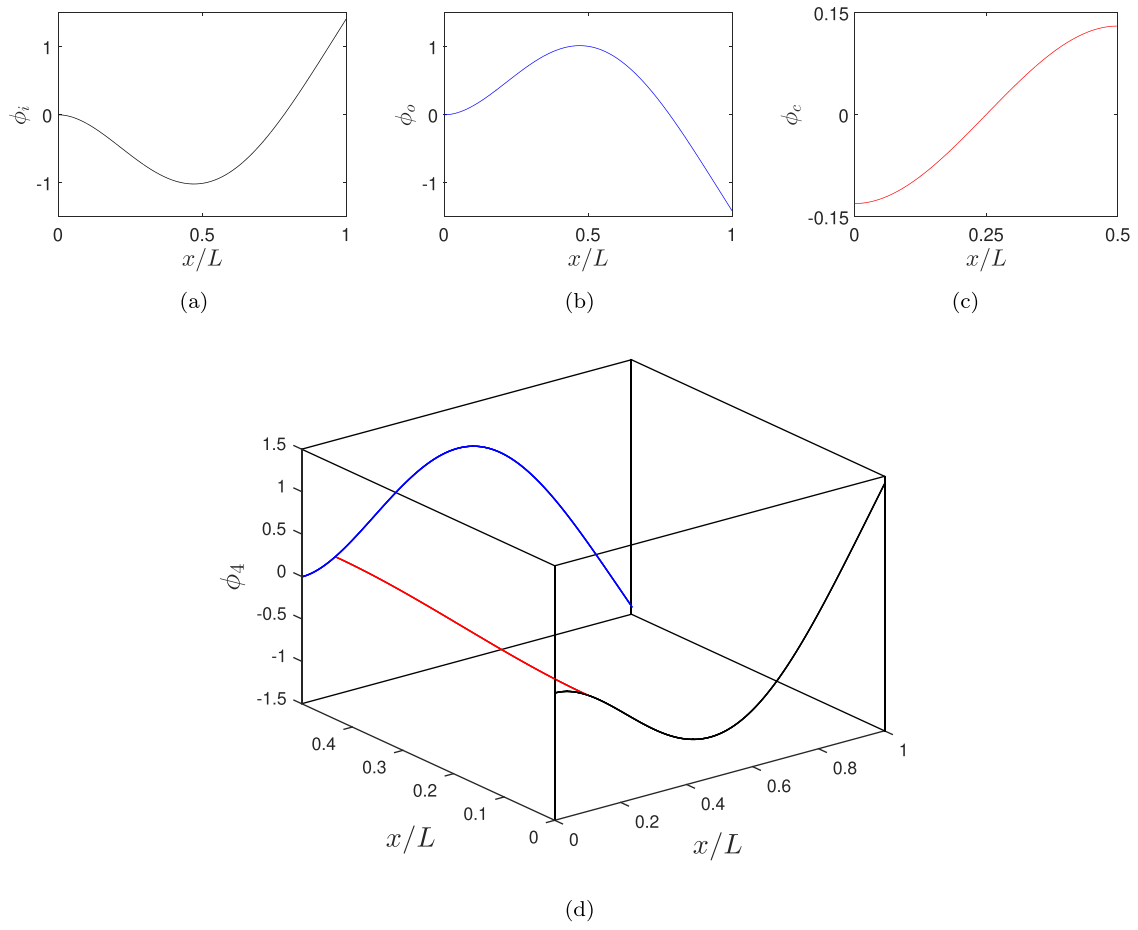

Fig. 5. Fourth mode shape of the mechanically-connected beams system of Fig. 1: mode shape of the (a) primary input beam, (b) primary output beam, (c) coupling beam, and (d) whole mechanical structure.

$$a_1 C_1 + a_2 C_5 = 0 \tag{20}$$

Depending on the value of the system natural frequency ω_n, one of the following two cases is observed for the constants' values a_1 and a_2:

1. If $a_1 = a_2$, then $C_1 = -C_5$ which makes the primary beams vibrate out-of-phase (anti-symmetric mode) with respect to each other.
2. If $a_1 = -a_2$, then $C_1 = C_5$ which makes the primary beams vibrate in-phase (symmetric mode) with respect to each other.

By setting one of the constants, C_1 in this case, equals to one, the numerical values for all of the C's in Eq. (17) can be found, and hence, their corresponding mode shape for the system natural frequency ω_n.

Normalization of mode shapes

Because the system of the algebraic equations, Eq. (16), is linear and homogeneous, then $\alpha\mathbf{C}$ is a solution of the algebraic equations given that the vector $\mathbf{C}$ is a solution and α is an arbitrary constant. Therefore, the mode shapes corresponding to the system natural frequency ω_n are unique for a certain constant, α. Hence, the mode shapes can then be normalized by setting

$$\int_{x_1}^{x_2} [\alpha\phi_n(x)]^2 dx = 1 \quad \text{or} \quad \alpha = \frac{1}{\sqrt{\int_{x_1}^{x_2} \phi_n^2(x) dx}} \tag{21}$$

where $\phi(x)$ is the mode shape associated with the system natural frequency ω_n. Finally, the topology of the considered structure, Fig. 1, and the reduced-order model analysis suggest that the constant α_r corresponding to the frequency ω_r and associating with the mode shape ϕ_r is given by

$$\alpha_r = \left(\int_o^{l_i} \phi_{i,1}^2(x) dx + \int_{l_i}^{1} \phi_{i,2}^2(x) dx + \int_o^{l_o} \phi_{o,1}^2(x) dx + \int_{l_o}^{1} \phi_{o,2}^2(x) dx + \frac{A_c}{A} \int_o^{l_c} \phi_c^2(x) dx \right)^{-1/2} \tag{22}$$

Results and discussion

The developed methodology is employed to study the mechanically-connected beam as shown in Fig. 1. Such system was used as micro filter that was fabricated and tested by Hammad et al. [21,22]. Table 1 lists the design parameters needed in the analysis of the considered mechanically-connected beam; the geometric dimensions and the material properties of the micro filter [21,22]. The input and output

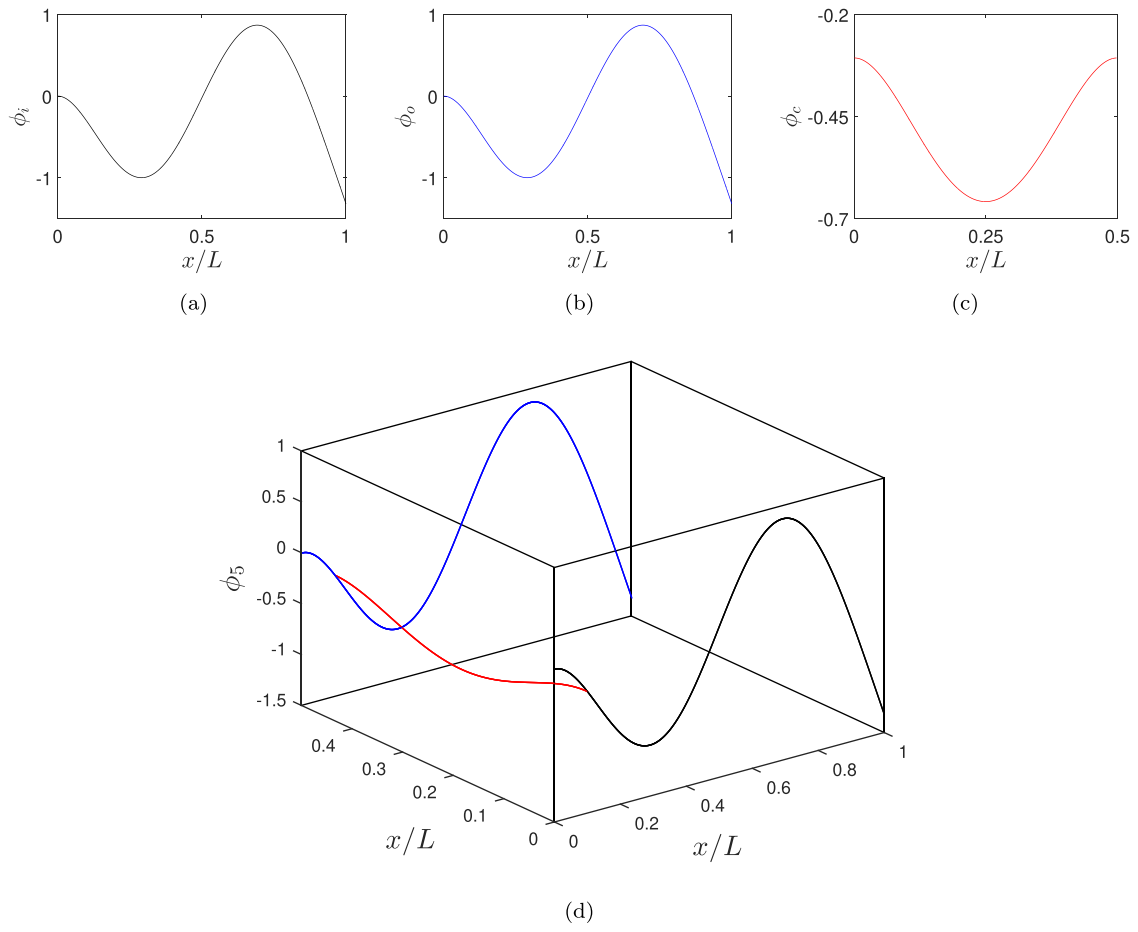

Fig. 6. Fifth mode shape of the mechanically-connected beams system of Fig. 1: mode shape of the (a) primary input beam, (b) primary output beam, (c) coupling beam, and (d) whole mechanical structure.

primary beams are coupled with the weak beam at $x = L_i = L_o = [4.08]\ \mu m$. The beams, primary and coupling, are made of Polysilicon material with a Young's modulus of $E = [150]\ GPa$ and a mass density of $\rho = [2300] kg/m^3$.

Closed-form expression of the mode shapes

In this section, the previously discussed methodology in the preceding sections was employed to find the closed-form expressions of the mode shapes for the mechanically-connected beams, Fig. 1. To avoid unnecessary repetition in obtaining higher mode shapes, only the first mode shape for the mechanical system with the specifications listed in Table 1 is considered. In this analysis, all the beams are assumed to be free of residual stresses; that is, no compressive axial loads $N_i = N_o = N_c = 0$.

The first nondimensional natural frequency of the mechanically-connected beams system, i.e., the corresponding smallest solution of the characteristic equation associated with $\det[\mathbf{M_r}] = 0$, is $\omega_1 = 3.515 = [1.489] MHz$. Upon substituting the numerical value of the fundamental natural frequency into the remaining boundary conditions, one can obtain $C_1 = C_5$, hence, a symmetric mode. By setting C_1 equals to one, the numerical values for all of the C's in Eqs. (17) can be found. Using the normalization condition given in Eq. (21), α_r was found to be $\alpha_r = 0.707$ and, hence, the following normalized closed-form expression of the first global mode shape for the mechanically-connected beams system is

$$\phi_{i,1}(x) = 0.707\{\cos[1.875x] - \cosh[1.875x]\} - 0.519\{\sin[1.875x] - \sinh[1.875x]\}, \quad \text{for } 0 < x < l_i \tag{23a}$$

$$\phi_{i,2}(x) = -0.707\{\cos[1.875(1-x)] - \cosh[1.875(1-x)]\} - 0.519\{\sin[1.875(1-x)] - \sinh[1.875(1-x)]\}, \quad \text{for} l_i < x < 1 \tag{23b}$$

$$\phi_{o,1}(x) = 0.707\{\cos[1.875x] - \cosh[1.875x]\} - 0.519\{\sin[1.875x] - \sinh[1.875x]\}, \quad \text{for } 0 < x < l_o \tag{23c}$$

$$\phi_{o,2}(x) = -0.707\{\cos[1.875(1-x)] - \cosh[1.875(1-x)]\} - 0.519\{\sin[1.875(1-x)] - \sinh[1.875(1-x)]\}, \quad \text{for} l_o < x < 1 \tag{23d}$$

$$\phi_c(x) = -0.011\cos[1.875x] - 0.0055\sin[1.875x] - 0.0127\cosh[1.875x] + 0.0055\sinh[1.875x], \quad \text{for } 0 < x < l_c \tag{23e}$$

Fig. 2 illustrates the first mode of the mechanically-connected beams system from the normalized expression defined in Eq. (23). In all mode shapes shown in the rest of the paper, the normalization scheme is used in the same way discussed above.

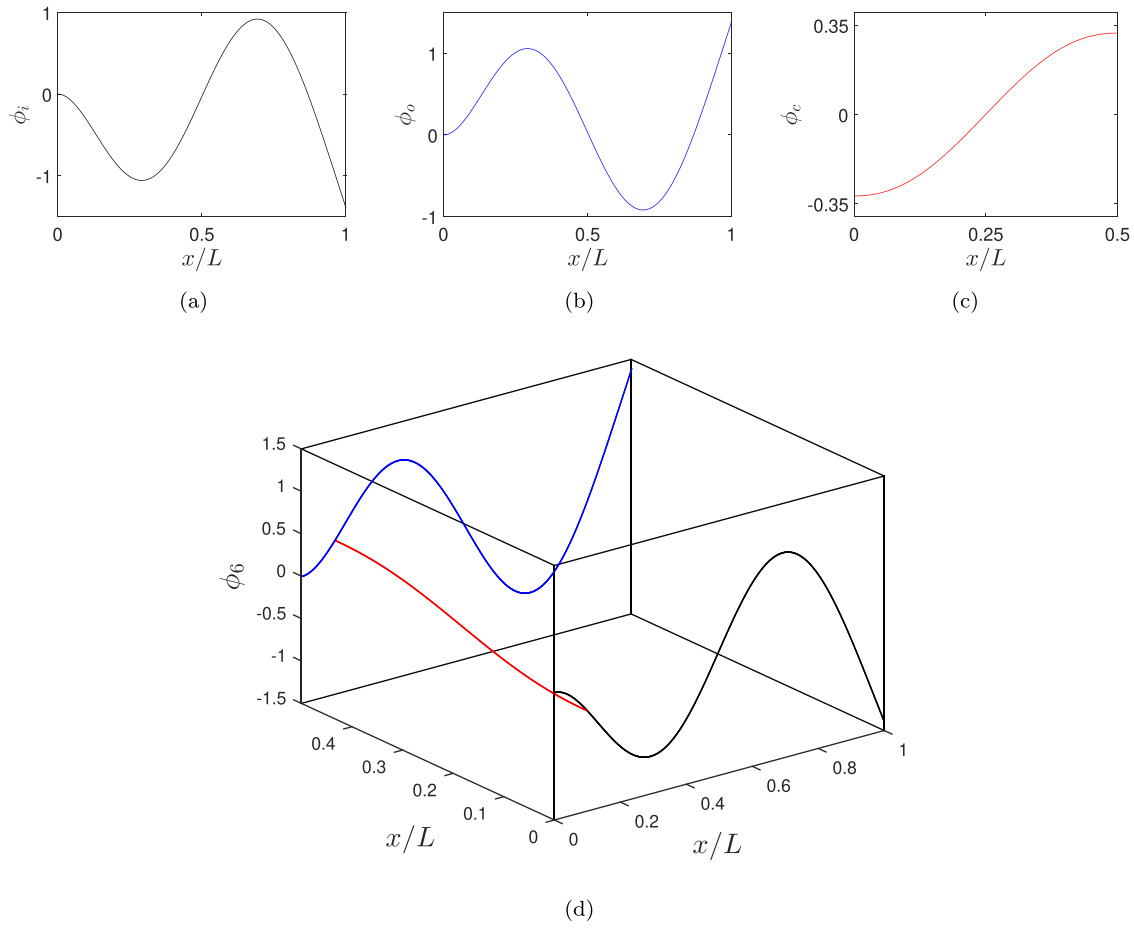

Fig. 7. Sixth mode shape of the mechanically-connected beams system of Fig. 1: mode shape of the (a) primary input beam, (b) primary output beam, (c) coupling beam, and (d) whole mechanical structure.

Validation of the results

In order to provide some results to compare with those obtained from the presented methodology of the mechanical system in Fig. 1, a finite element analysis (FEA) using ANSYS (ANSYS, Inc, Academic Research, Release 16.2, 2015) and COMSOL multiphysics were prepared for validation purpose. A three-dimensional 10-node tetrahedral structural solid element SOLID187 was employed. This element has a quadratic displacement behavior and is well suited to modeling irregular meshes. Each node of the 10-nodes has three degree of freedoms; only translation motions in x, y and z directions. Reference [32] contains additional details of the ANSYS and COMSOL employed models, the solution analyses and the associated results. Using the modal analysis approach, the analytically-determined and the numerically-predicted natural frequencies of the mechanically-connected beams system are listed in Table 2. The natural frequencies were obtained in Hz from the nondimensional natural frequency, ω, using the following relation

$$f = \frac{\omega}{2\pi T} \quad \text{where } T = \sqrt{\frac{\rho A L^4}{EI}} \tag{23f}$$

where in case of the parameters given in Table 1, the time value is $T = 3.758 \times 10^{-7}$ s. Inspecting the results in Table 2, the analytically-determined natural frequencies obtained from the proposed analytical approach in this paper agree very well with the numerically-predicted natural frequencies from the numerical approaches; ANSYS and COMSOL. The excellent agreement is supported by the small percentage difference error that is less than 2 %. Furthermore, the mode shapes of the mechanically-connected beams system obtained from the proposed approach, whether being in-phase or out-of-phase, and their order, are in complete agreement with the ones obtained from the FEM. Reference [32] also contains additional results using different coupling positions; $l_i = l_o = 10$ % (considered here), 20 %, 50 %, and 80 % away from clamped-end. Even though the FE solution (ANSYS and COMSOL) provides all the frequencies and mode shapes of the mechanical system (transverse motion, torsional motion, axial motion, or a combination of these motions), only the frequencies and mode shapes in the transverse motion are considered here.

Mode shapes

The first and second global mode shapes of the mechanically-connected beams system of Fig. 1 are illustrated in Figs. 2 and 3, respectively. As stated previously, the primary input and output beams are oscillating in-phase in the first mode, Fig. 2. However, the primary beams are oscillated out-of-phase in the second mode, Fig. 3. It is worthwhile to mention that both of the input and output primary beams in their first and second mode shapes vibrate in a similar way as the first mode of a single clamped-free (cantilever) beam.

The third and fourth global mode shapes of the mechanically-connected beams system of Fig. 1 are depicted in Figs. 4 and 5, respectively. The primary input and output beams are oscillating in-phase in the third mode, Fig. 4, and out-of-phase in the fourth mode, Fig. 5. Both of the input and output primary beams in their third and fourth mode shapes vibrate in a similar way as the second mode of a clamped-free beam. There is a node as shown in Figs. 4 and 5 at a distance $x/L \approx 0.8$.

The fifth and sixth global mode shapes of the mechanically-

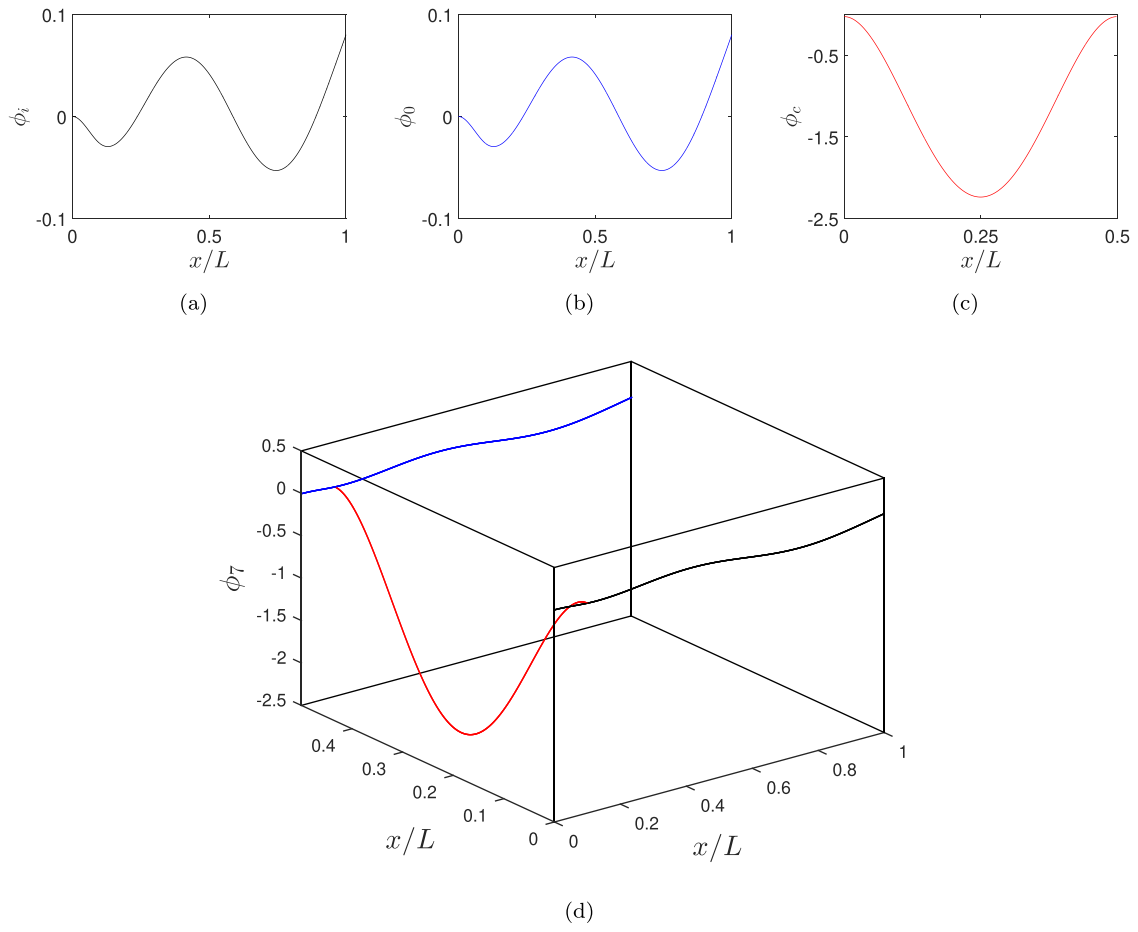

Fig. 8. Seventh mode shape of the mechanically-connected beams system of Fig. 1: mode shape of the (a) primary input beam, (b) primary output beam, (c) coupling beam, and (d) whole mechanical structure.

connected beams system of Fig. 1 are shown in Figs. 6 and 7, respectively. The primary input and output beams are oscillating in-phase in the fifth mode, Fig. 6, and out-of-phase in the sixth mode, Fig. 7. Both of the primary beams in their fifth and sixth mode shapes vibrate in a similar way as the third mode of a cantilever beam. There are two nodes as shown in Figs. 6 and 7 which are located at a distance $x/L \approx 0.5$ and 0.8. The vibration amplitudes of the primary beams are much higher (approximately 5 times) than the amplitude of the coupling beam for the previous mode shapes, Figs. 2 to 7.

Fig. 8 shows the seventh global mode shape of the mechanically-connected beams system of Fig. 1. For the given dimensions of the primary and coupling beams in Table 1, there is a mode shape after the sixth one in which the vibrations of the coupling beam are dominant, i.e., the vibrations of input and output primary beams are very small compared to the coupling beam vibrations. This means that the seventh mode corresponds to the first mode of the coupling beam oscillation. The mode resemble to a mode of a single beam with slightly flexible clamping points (finite rigidity of the clamping points). The seventh natural frequency comes between the two coupled frequencies namely, the fifth and sixth (61.45 and [61.65]rad/s) and the eighth and ninth (120.46 and [121.33]rad/s). The modes appear at relatively high frequencies due to our model focusing on transverse vibrations of the beams, meaning the vibrations are perpendicular to the plane containing the primary input, the primary output, and the coupling beams. Since the flexural stiffness EI of the coupling beam in the in-plane direction is about six times smaller than in the transverse direction, the in-plane modes have lower frequencies. However, because the model assumes transverse base actuation, the in-plane modes are not activated, justifying the use of a transverse-vibration model exclusively.

Coupling location

The effects of changing coupling (attachment) location on the natural frequencies of the mechanical system of Fig. 1 are investigated. The values of the natural frequencies are studied to observe the general behavior of the frequencies as the attachment point is changing. The variations of natural frequencies of the first and second modes, third and fourth modes, and fifth and sixth modes with respect to the coupling positions are illustrated in Fig. 9(a), (b), and (c) respectively.

Fig. 9(a) shows the variation of the first and second natural frequencies with coupling position. Both frequencies start around 3.5 MHz. Even though the value of the first natural frequency does not change with the coupling position, the second natural frequency increases rapidly to reach a value 2.5 times of the initial value. The variations of the third and fourth natural frequencies with the coupling position are depicted in Fig. 9(b). The difference of the third and fourth natural frequencies which is an indicator of actual bandwidth of the system is increasing as the coupling location approaches to the center of the primary beams and decreases to zero at $x/L = 0.8$ and then increasing again. The effect of changing the attachment location of the coupling beam to the primary beams on the fifth and sixth natural frequencies is shown in Fig. 9(c).

Coupling lengths

The effect of changing beam length, L_c, on the natural frequencies of the mechanical system in Fig. 1 is depicted in Fig. 10 for different coupling beam location. For the previous analyses, the coupling beam was positioned at a distance $L_i = L_o = 10$ % of the primary beam length,

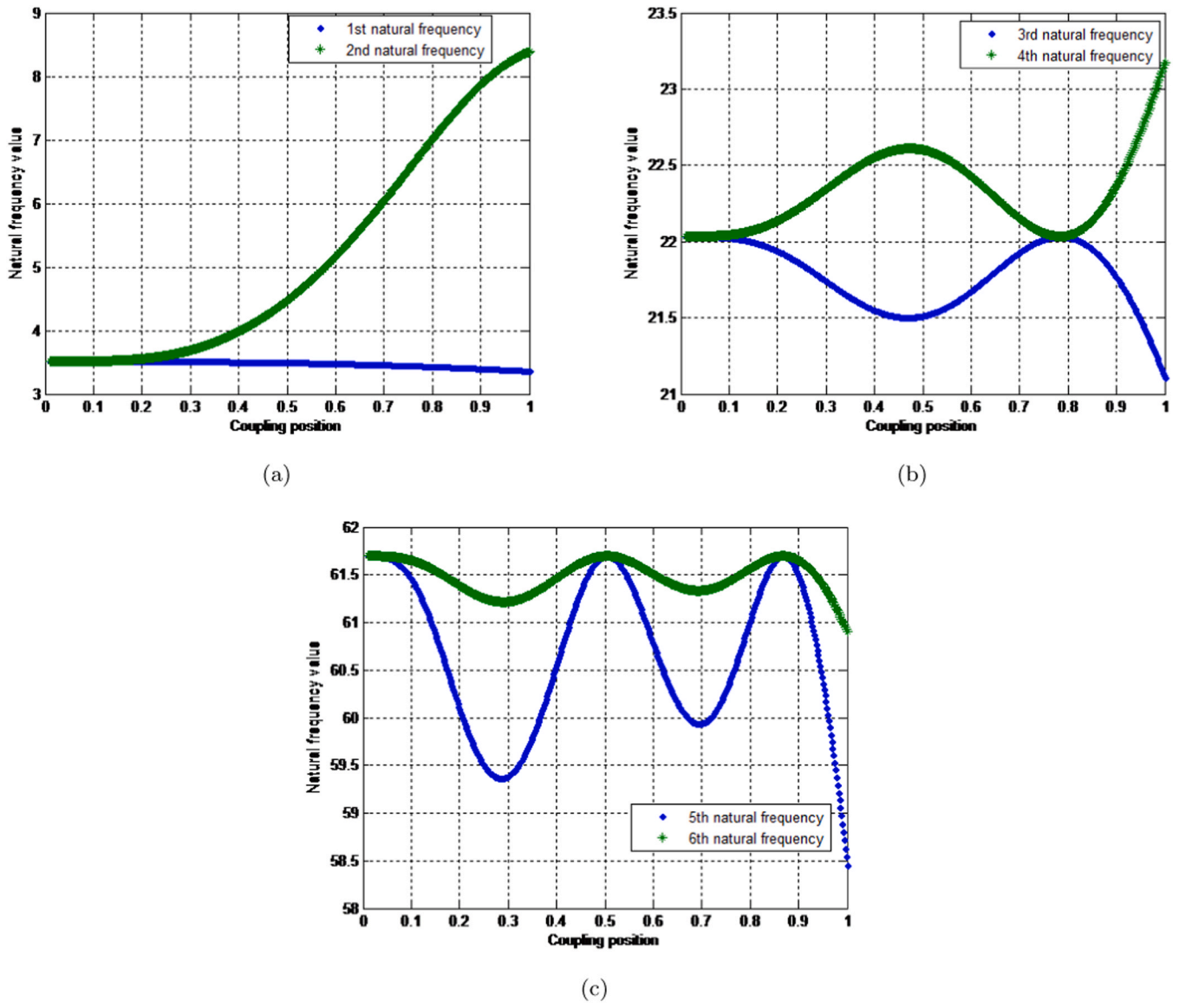

Fig. 9. Variations of the (a) first and second (b) third and fourth (c) fifth and sixth natural frequencies of the mechanically-connected beams system of Fig. 1 with the attachment location.

L, away from clamped-end, i.e., $L_i = L_o = 0.1L = [4.08]\mu m$. The coupling beam now is placed at different locations away from the clamped ends and its length was varied from $L_c = 0.005\ \%L$ to $50\ \%L$ as illustrated in Fig. 10.

Fig. 10(a) shows the variations of the lowest six natural frequencies with the coupling beam length, L_c, when the coupling beam was placed $10\ \%L$ away from the clamped end. The first, third, and fifth natural frequencies remain unchanged as the coupling beam length is varying. The other natural frequencies are decreasing with the increasing of the coupling beam length. The differences between the first and second, third and fourth, and fifth and sixth natural frequencies decrease as the coupling length increases till both values of the two successive frequencies approach each other. When the coupling beam was placed $20\ \%L$ away from the clamped-end, the variations of the natural frequencies with respect to the coupling beam length is illustrated in Fig. 10(b). The same behavior is observed except that the differences between two successive frequencies become larger. When the coupling beam was placed $40\ \%L$ away from the clamped ends, Fig. 10(c) shows the same behavior as the ones discussed previously in Figs. 10(a) and (b).

Fig. 10(d) and (e) show an interesting behavior when the coupling beam is placed $50\ \%L$ and $80\ \%L$ away from the clamped ends. The attachment points, $L_c = 50\ \%L$ and $80\ \%L$, are nodes which occur at the fifth and sixth and third and fourth mode shapes as shown in Figs. 6 and 7 and 4 and 5, respectively. As shown in Fig. 10(d), the fourth and the fifth natural frequencies have almost identical values when $L_c < 0.1L$. Whence $L_c \approx 0.1L$, the three natural frequencies, i.e., forth, fifth, and sixth, have the same values (crossing each other). The Fig. 10(d) shows that beyond this point the fourth natural frequency will decrease as the coupling beam length increasing. However, from a practical point of view, the sixth natural frequency is the one that will decrease when it crosses the point $L_c = 10\ \%L$ where the other natural frequencies will remain unchanged with the increasing of the coupling beam length. The same concept is applied to the behavior in Fig. 10(e) where the second and the third natural frequencies have identical values when $L_c < 0.2L$. Whence $L_c \approx 0.2L$, the three natural frequencies, i.e., second, third, and forth, have the same values. This means that there are three coupled frequencies when $L_i = L_o = 50\ \%L$ and $L_c = 0.1L$ and when $L_i = L_o = 80\ \%L$ and $L_c = 0.2L$. Fig. 10(e) shows that beyond this point the second natural frequency will decrease as the coupling beam length increasing.

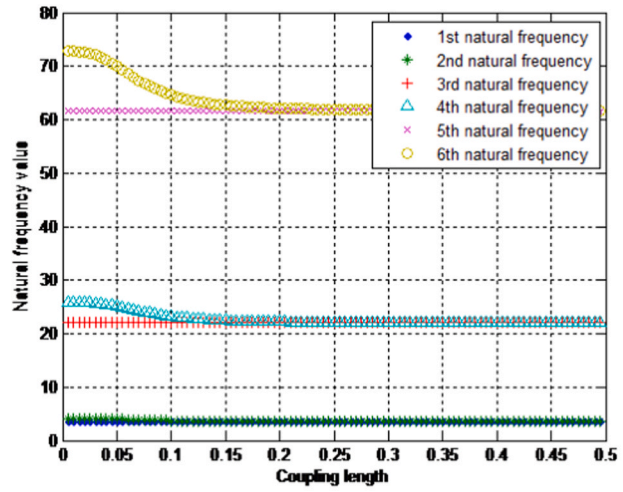

(a) 10%

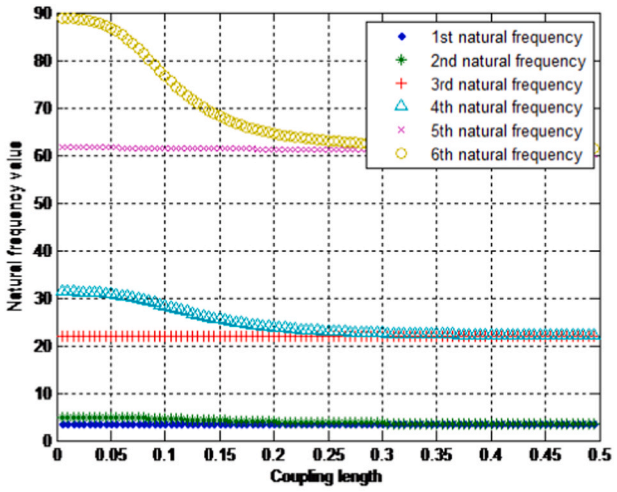

(b) 20%

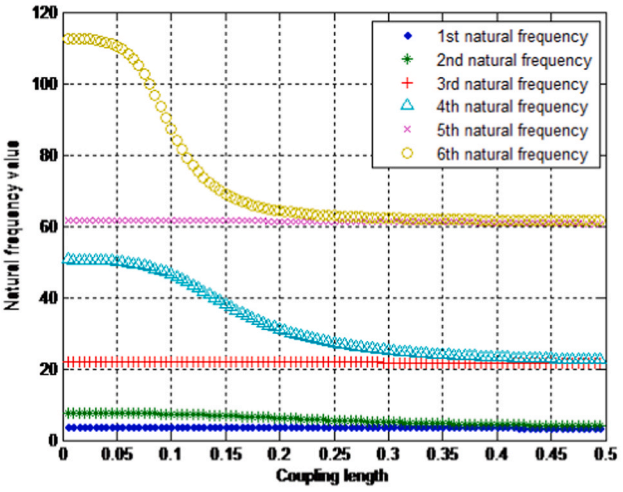

(c) 40%

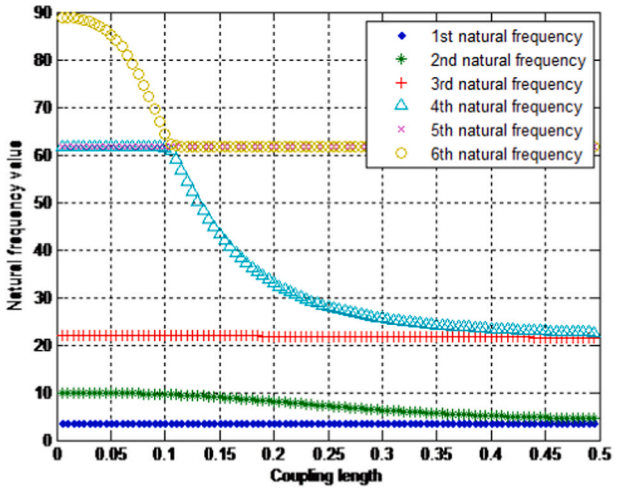

(d) 50%

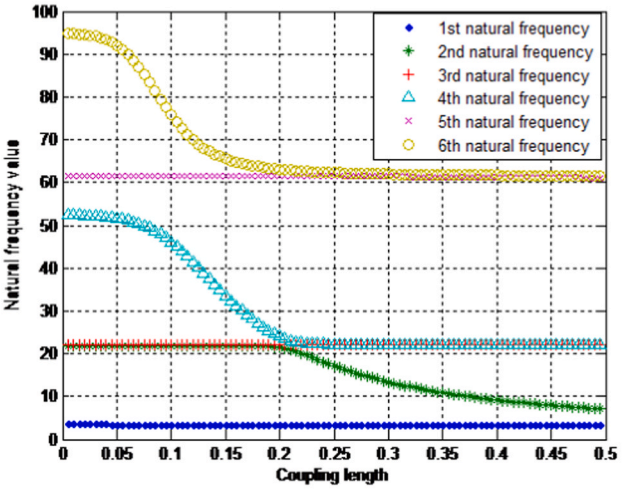

(e) 80%

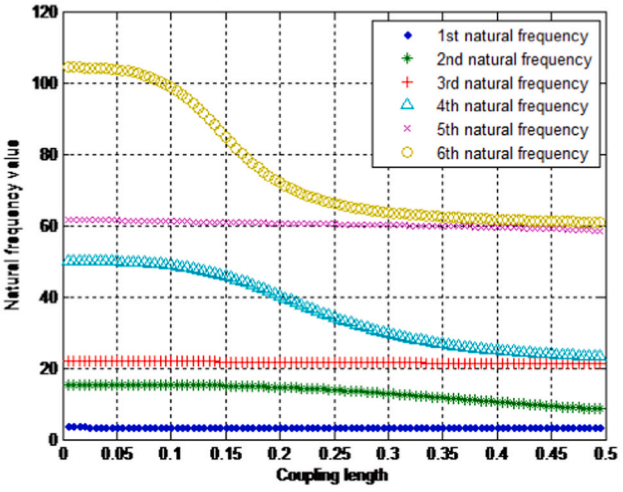

(f) 100%

Fig. 10. Variation of the lowest six natural frequencies of the mechanically-connected beams system shown in Fig. 1 with respect to the coupling beam length, at coupling position (a) 10 %, (b) 20 %, (c) 40 %, (d) 50 %, (e) 80 % and (f) 100 % away from clamped-end.

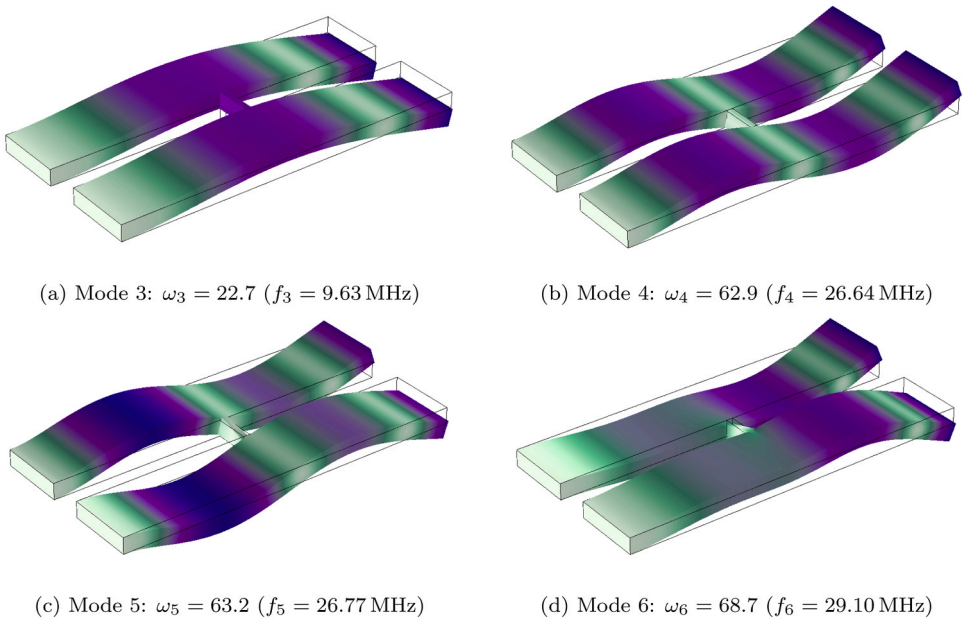

(a) Mode 3: $\omega_3 = 22.7$ ($f_3 = 9.63$ MHz) (b) Mode 4: $\omega_4 = 62.9$ ($f_4 = 26.64$ MHz)

(c) Mode 5: $\omega_5 = 63.2$ ($f_5 = 26.77$ MHz) (d) Mode 6: $\omega_6 = 68.7$ ($f_6 = 29.10$ MHz)

Fig. 11. The corresponding (a) third, (b) fourth, (c) fifth, and (d) sixth mode shapes of the mechanically-connected beams system of Fig. 1 with attachment points at $L_i = L_o = 50\ \%L = [20.4]\mu m$ and a coupling beam length of $L_c = 10\ \%L = [4.08]\mu m$.

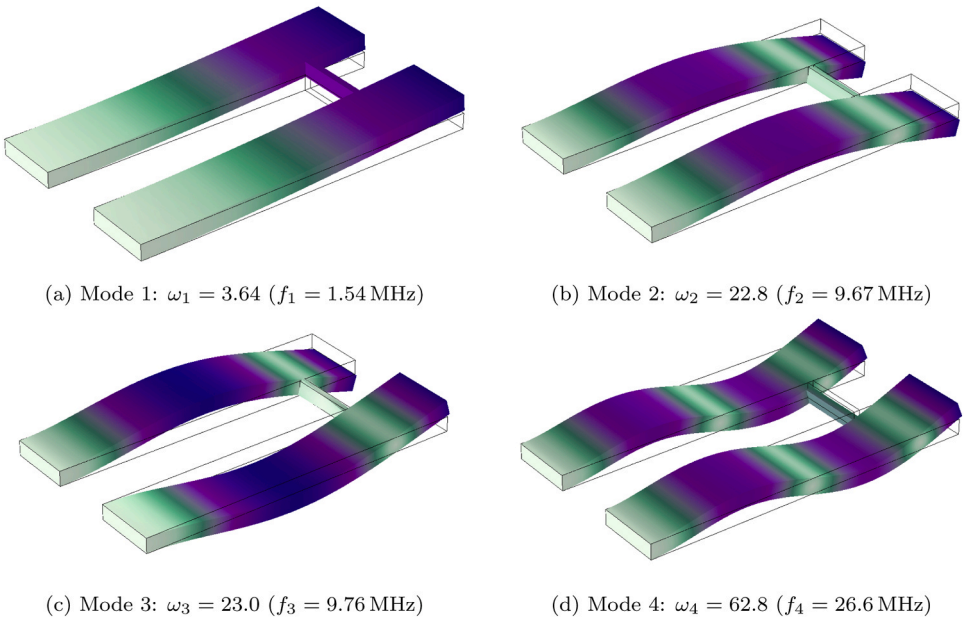

(a) Mode 1: $\omega_1 = 3.64$ ($f_1 = 1.54$ MHz) (b) Mode 2: $\omega_2 = 22.8$ ($f_2 = 9.67$ MHz)

(c) Mode 3: $\omega_3 = 23.0$ ($f_3 = 9.76$ MHz) (d) Mode 4: $\omega_4 = 62.8$ ($f_4 = 26.6$ MHz)

Fig. 12. The corresponding (a) first, (b) second, (c) third, and (d) fourth mode shapes of the mechanically-connected beams system of Fig. 1 with attachment points at $L_i = L_o = 80\ \%L = [32.64]\mu m$ and a coupling beam length of $L_c = 20\ \%L = [8.16]\mu m$.

However, from a practical point of view, the fourth natural frequency is the one it will decrease when it crosses the point $L_c = 20\ \%L$ where the other natural frequencies will remain unchanged with the increasing of the coupling beam length.

Fig. 10(f) shows the variation of the first six natural frequencies when the coupling beam is attached at the free-ends. When the coupling beam length was increased, the value of the second natural frequency approaches the first natural frequency and so the forth and sixth frequencies approach the third and fifth ones, respectively. The position and/or the length of the coupling beam has a major impact on the natural frequencies of the mechanically-connected beams system shown in Fig. 1. The values of the natural frequencies can change widely and thus can be used to enhance the dynamics of beams. Reference [32] contains additional figures for different coupling beam locations.

To understand how the mechanically-connected beams system of Fig. 1 behave in the crossing points of Fig. 10(d) and 10(e), the third, fourth, fifth, and sixth mode shapes of the considered system when the coupling beam of a corresponding length of $L_c = 10\ \%L = [4.08]\mu m$ is attached to the primary beams at $L_i = L_o = 50\ \%L = [20.4]\mu m$ are shown in Fig. 11. The mode shapes were obtained using the COMSOL multiphysics software for better visualization. It is clear that the third mode in Fig. 11 is similar to the third mode of Fig. 4. However, the fourth mode in Fig. 11 is similar to the fifth mode of Fig. 6, where the fourth mode of Fig. 5 cannot be excited. Fig. 12 shows the first, second, third, and fourth mode shapes of the mechanically-connected beams system of Fig. 1 with attachment points at $L_i = L_o = 80\ \%L = [32.64]\mu m$ and a coupling beam

length of $L_c = 20\ \%L = [8.16]\mu m$. Even though the first mode shape in Fig. 12 looks similar to the first mode shape of Fig. 2, the second mode of Fig. 3 was not excited as illustrated in Fig. 12. Therefore, the phenomenon corresponding to the crossing of mode shapes is observed when the weak beam is coupled to one of the nodes of the lower modes.

Conclusions

The natural frequencies and mode shapes of a linear, undamped, and unforced vibration problem of mechanically-connected beams system shown in Fig. 1 were obtained in closed-from expressions. The equations of motion of the connected beams were derived using Galerkin's discretization method. The boundary value problem (BVP) of the mechanically-connected beams system was consisted of five partial differential equations and twenty boundary and continuity conditions. Rather than solving a large and costly system of linear homogeneous algebraic equations, the problem was reduced to a set of three equations with three unknown constants and the corresponding system natural frequencies. This approach mathematically saves time and cost when dealing with a smaller system and makes the relation between the parameters of the mechanically-connected beams system clearer to understand. The characteristic equation from which the natural frequencies were solved was obtained by setting the determinant of the reduced coefficient matrix equal to zero. This equation was then solved numerically to find the natural frequencies and mode shapes. The presented methodology was validated by comparing the obtained analytical solution with the finite-element results. The closed-form expressions derived in this work are more easily-handled, robust, and accurate compared to the FEM approach. The analytical approach is beneficial for developing reduced-order models of the nonlinear static and dynamic behavior of mechanical systems using the Galerkin procedure.

The natural frequency of the single resonator splits into two closely spaced frequencies in the system: one corresponding to an in-phase mode and the other to an out-of-phase mode. Moreover, the effects of the attachment point and coupling beam length on the natural frequencies of the connected beams were also discussed. When the coupling beam is attached at the middle of the resonator beams, i.e., 50 % away from clamped-ends, three natural frequencies meet at a point when the length of the coupling is $L_c = 10\ \%$ of the primary beams length. A similar phenomenon was observed when the coupling beam was placed 80 % away from the clamped-ends. Finally, although the vibration model presented in this paper is limited to a mechanically-connected system composed of two clamped-free beams, it can be easily modified and adapted to model with any array of mechanically coupled beams.

CRediT authorship contribution statement

Abdulaziz Alazmi: Writing – review & editing, Writing – original draft, Visualization, Validation, Software, Methodology, Investigation, Formal analysis, Data curation. **Abdullah Alshaya:** Writing – review & editing, Visualization, Validation, Software, Methodology, Investigation, Formal analysis. **Khaled Alhazza:** Writing – review & editing, Writing – original draft, Supervision, Project administration, Methodology, Formal analysis, Conceptualization.

Funding

This research received no specific grant from any funding agency in the public, commercial, or not-for-profit sectors.

Declaration of Competing Interests

The authors declare that they have no known competing financial interests or personal relationships that could have appeared to influence the work reported in this paper.

Data availability

The data used to support the findings as well as the finite-element model are available from the corresponding author upon reasonable request.

References

[1] S. Moaveni. Finite Element Analysis Theory and Application with ANSYS, 3rd edition, Pearson Prentice Hall, New Jersey, 2008.
[2] M. Hajianmaleki, M.S. Qatu, Vibrations of straight and curved composite beams: a review, Compos. Struct. 100 (2013) 218–232.
[3] I.H. Shames, C.L. Dym, Energy and Finite Element Methods in Structural Mechanics, McGraw-Hill, New York, 1985.
[4] L. Meirovitch, Analytical Methods in Dynamics, Macmillan, New York, 1967.
[5] S. Timoshenko, On the correction for shear of the differential equation for transverse vibrations of prismatic bars, Philos. Mag. J. Sci. 41 (1921) 744–747.
[6] S. Timoshenko, On the transverse vibrations of bars of uniform cross-section, Philos. Mag. J. Sci. 43 (1922) 125–139.
[7] P. Malatkar, Nonlinear Vibrations of Cantilever Beams and Plates, Ph.D. thesis, Virginia Polytechnic Institute and State University, Blacksburg, Virginia, 2003.
[8] K.A. Alhazza, A.A. Alhazza, A review of the vibrations of plates and shells, volume 36 of The Shock and vibration digest, Sage, Thousand Oaks, CA, 2004.
[9] S. Woinowsky-Krieger, The effect of an axial force on the vibration of hinged bars, J. Appl. Mech. 17 (1950) 35–36.
[10] D. Burgreen, Free vibrations of a pin-ended column with constant distance between pin ends, J. Appl. Mech. 18 (1951) 135–139.
[11] D.A. Evensen, Nonlinear vibrations of beams with various boundary conditions, AIAA J. 6 (1968) 370–372.
[12] V.V. Bolotin, The Dynamic Stability of Elastic Systems, Holden-Day, San Francisco, California, 1964.
[13] S. Atluri, Nonlinear vibrations of a hinged beam including nonlinear inertia effects, J. Appl. Mech. 40 (1973) 121–126.
[14] M.R.C. da Silva, Flexural-flexural oscillations of beck's column subject to a planar harmonic excitation, J. Sound Vib. 60 (1978) 133–144.
[15] M.R.C. da Silva, Harmonic non-linear response of beck's column to a lateral excitation, Int. J. Solids Struct. 14 (1978) 987–997.
[16] P.F. Pai, A.H. Nayfeh, Non-linear non-planar oscillations of a cantilever beam under lateral base excitations, Int. J. Non-Linear Mech. 25 (1990) 455–474.
[17] M.R.C. daSilva, C.L. Zaretzky, Nonlinear dynamics of a flexible beam in a central gravitational field-i equations of motion, Int. J. Solids Struct. 30 (17) (1993) 2287–2299.
[18] S.M. Han, H. Benaroya, T. Wei, Dynamics of transversely vibrating beams using four engineering theories, J. Sound Vib. 225 (5) (1999) 935–988.
[19] H.N. Arafat, Nonlinear Response of Cantilever Beams, Ph.D. thesis, Virginia Polytechnic Institute and State University, Blacksburg, Virginia, 1999.
[20] S.A. Emam, A Theoretical and Experimental Study of Nonlinear Dynamics of Buckled Beams, Ph.D. thesis, Virginia Polytechnic Institute and State University, Blacksburg, Virginia, 2002.
[21] B.K. Hammad, Modeling, Simulation, and Analysis of Micromechanical Filters Coupled with Capacitive Transducers, Ph.D. thesis, Virginia Polytechnic Institute and State University, Blacksburg, Virginia, 2008.
[22] B.K. Hammad, Natural frequencies and mode shapes of mechanically coupled microbeam resonators with an application to micromechanical filters, Shock Vib. 2014 (2014) 939467.
[23] Y. Gurbuz, M. Parlak, T.F. Bechteler, A. Bozkurt, An analytical design methodology for microelectromechanical (mem) filters, Sens. Actuators A: Phys. 119 (1) (2005) 38–47.
[24] H. Ding, G.C. Zhang, L.Q. Chin, Supercritical vibration of nonlinear coupled moving beams based on discrete fourier transform, Int. J. Non-Linear Mech. 47 (2012) 1095–1104.
[25] S.S. Arora, Study of Vibration Characteristics of Cantilever Beams of Different Materials, Master's thesis, Thapar University, Patiala, India, 2012.
[26] J. Ma, Y. Chen, W. Wu, et al., Dynamic modeling and resonant analysis of rotating internally connected laminated piezoelectric beams, Acta Mech. 235 (2024) 355–368.
[27] K. Kim, P. Han, K. Jong, C. Jang, R. Kim, Natural frequency calculation of elastically connected double-beam system with arbitrary boundary condition, AIP Adv. 10 (2020) 055026.
[28] A. Azizzadeh, B. Behjat, Static and natural frequency investigation of fgp beams considering thermal effects and design parameters, J. Eng. Appl. Sci. 70 (2023) 92.
[29] M. Liu, G. Yao, Nonlinear forced vibration and stability of an axially moving beam with a free internal hinge, Nonlinear Dyn. 112 (2024) 6877–6896.
[30] T. Rabenimanana, M. Ghommem, et al., On the equivalence between mass perturbation and dc voltage bias in coupled mems resonators: Theoretical and experimental investigation, J. Appl. Phys. 10 (2022) 055026.
[31] F. Najar, M. Ghommem, T. Rabenimanana, M. Hemid, V. Walter, N. Kacem, Differential capacitive mass sensing based on mode localization in coupled microbeam arrays, Mech. Syst. Signal Process. 220 (2024) 111648.
[32] A.H. Alduwahis, Dynamics of connected Beams, Master's thesis, Kuwait University, Kuwait, Kuwait, 2014.